

# Subwavelength plasmonic waveguide structures based on slots in thin metal films

Georgios Veronis and Shanhui Fan

Department of Electrical Engineering, Stanford University, Stanford, California 94305

## ABSTRACT

We demonstrate the existence of a bound optical mode supported by an air slot in a thin metallic film deposited on a substrate, with slot dimensions much smaller than the wavelength. The modal size is almost completely dominated by the near field of the slot. Consequently, the size is very small compared with the wavelength, even when the dispersion relation of the mode approaches the light line of the surrounding media. In addition, the group velocity of this mode is close to the speed of light in the substrate, and its propagation length is tens of microns at the optical communication wavelength. We also investigate the performance of bends and power splitters in plasmonic slot waveguides. We show that, even though the waveguides are lossy, bends and splitters with no additional loss can be designed over a wavelength range that extends from DC to near-infrared, when the bend and splitter dimensions are much smaller than the propagation length of the optical mode. We account for this effect with an effective characteristic impedance model based upon the real dispersion relation of the plasmonic waveguide structures.

**Keywords:** Plasmonic devices, subwavelength optical devices, bends, splitters

## 1. INTRODUCTION

In this paper we demonstrate the existence of a bound plasmonic mode supported by a slot in a thin metallic film deposited on a substrate, with slot dimensions much smaller than the wavelength. We also show that bends and splitters in slot-based waveguides can be designed to have no additional loss over a wavelength range that extends from DC to near-infrared, when the bend and splitter dimensions are much smaller than the propagation length of the optical mode. We use frequency-domain techniques for the modeling of these plasmonic devices.

The dielectric constant of metals at optical wavelengths is complex, i.e.  $\epsilon_r(\omega) = \epsilon_{\text{Re}}(\omega) + i\epsilon_{\text{Im}}(\omega)$  and is a complicated function of frequency.<sup>1</sup> Thus, several simulation techniques which are limited to lossless, non-dispersive materials are not applicable to plasmonic devices. In time-domain methods the dispersion properties of metals have to be approximated by suitable analytical expressions.<sup>2</sup> In most cases the Drude model is invoked to characterize the frequency dependence of the metallic dielectric function<sup>3</sup>

$$\epsilon_{r,\text{Drude}} = 1 - \frac{\omega_p^2}{\omega(\omega + i\gamma)} \quad (1)$$

where  $\omega_p$ ,  $\gamma$  are frequency-independent parameters. However, the Drude model approximation is valid over a limited wavelength range. The range of validity of the Drude model can be extended by adding Lorentzian terms to Eq. (1) to obtain the Lorentz-Drude model<sup>3</sup>

$$\epsilon_{r,\text{LD}} = \epsilon_{r,\text{Drude}} + \sum_{j=1}^k \frac{f_j \omega_j^2}{(\omega_j^2 - \omega^2) - i\omega\gamma_j} \quad (2)$$

where  $\omega_j$  and  $\gamma_j$  stand for the oscillator resonant frequencies and bandwidths respectively, and  $f_j$  are weighting factors. Physically, the Drude and Lorentzian terms are related to intraband (free-electron) and interband (bound-electron) transitions respectively.<sup>3</sup> Even though the Lorentz-Drude model extends the range of validity of analytical approximations to metallic dielectric constants, it is not suitable for description of sharp absorption edges observed in some metals, unless a very large number of terms is used. In particular, the Lorentz-Drude model cannot approximate well the onset of interband absorption in noble metals (Ag, Au, Cu) even if five Lorentzian terms are used.<sup>3</sup> In Fig. 1 we compare the Drude and Lorentz-Drude models with experimental data

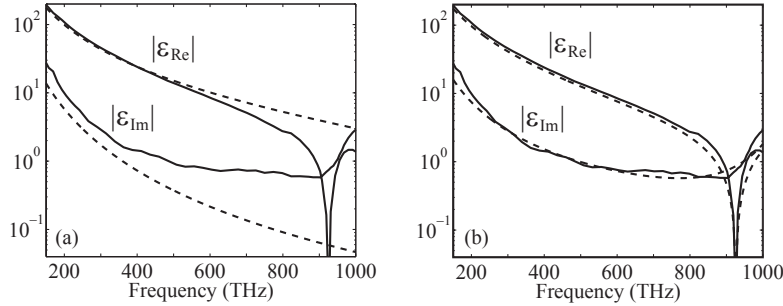


**Figure 1.** Real and imaginary part of the dielectric constant of silver at optical frequencies. The solid lines show experimental data. The dashed lines show values calculated using (a) the Drude model, (b) the Lorentz-Drude model with five Lorentzian terms. The parameters of the models are optimal and obtained through an optimization procedure.

for silver. We observe that even a five-term Lorentz-Drude model with optimal parameters results in a factor of two error at certain frequencies. As a result, broadband time-domain simulations can give accurate results in a limited wavelength range. Frequency-domain techniques are more suitable for modeling of plasmonic metallic devices, since they can treat arbitrary material dispersion.

## 2. GUIDED SUBWAVELENGTH PLASMONIC MODE SUPPORTED BY A SLOT IN A THIN METAL FILM

Waveguide structures which support highly-confined optical modes are important for achieving compact integrated photonic devices.<sup>4,5</sup> In particular, plasmonic waveguides have shown the potential to guide subwavelength optical modes. Several different plasmonic waveguiding structures have been proposed.<sup>4,6-15</sup> However, these structures support a highly-confined mode only near the surface plasmon frequency. In this regime, the optical mode typically has low group velocity and short propagation length.

Here we investigate the characteristics of the bound optical mode supported by an air slot in a thin metallic film deposited on a substrate (inset of Fig. 2a). This structure is hereafter referred to as a plasmonic slotline. Of particular interest is the regime where the dimensions of the slot are much smaller than the wavelength. We show that such a structure supports a fundamental bound mode with size almost completely dominated by the near field of the slot over a wide range of frequencies. The size of this mode can be far smaller than the wavelength even when its effective index approaches that of the substrate. In addition, the group velocity of the mode is close to the speed of light in the substrate and its propagation length is tens of microns at the optical communication wavelength. Thus, such a waveguide could be potentially important in providing an interface between conventional optics and subwavelength electronic and optoelectronic devices.

### 2.1. Finite-difference frequency-domain mode solver

We calculate the eigenmodes of the plasmonic slotline at a given wavelength  $\lambda_0$  using a full-vectorial finite-difference frequency-domain (FDFD) mode solver. For waveguiding structures which are uniform in the  $z$  direction, if an  $\exp(-\gamma z)$  dependence is assumed for all field components, Maxwell's equations reduce to two coupled equations for the transverse magnetic field components  $H_x$  and  $H_y$ .<sup>16</sup> These equations are discretized on a non-uniform orthogonal grid resulting in a sparse matrix eigenvalue problem of the form  $\mathbf{A}\mathbf{h} = \gamma^2\mathbf{h}$ , which is solved using iterative sparse eigenvalue techniques.<sup>17</sup> To calculate the bound eigenmodes of the waveguide, we ensure that the size of the computational domain is large enough so that the fields are negligibly small at its boundaries,<sup>18</sup> while for leaky modes we use perfectly matched layer absorbing boundary conditions.<sup>17</sup> An important feature of this formulation is the absence of spurious modes.<sup>18</sup> In addition, the frequency-domain mode solver allows us to directly use experimental data for the frequency-dependent dielectric constant of metals,<sup>1</sup> including both the real and imaginary parts, with no further approximation. We define here the propagation length  $L_p$  and the effective index  $n_{\text{eff}}$  of a propagating mode through the equation  $\gamma \equiv L_p^{-1} + i\beta = L_p^{-1} + i2\pi n_{\text{eff}}\lambda_0^{-1}$ .

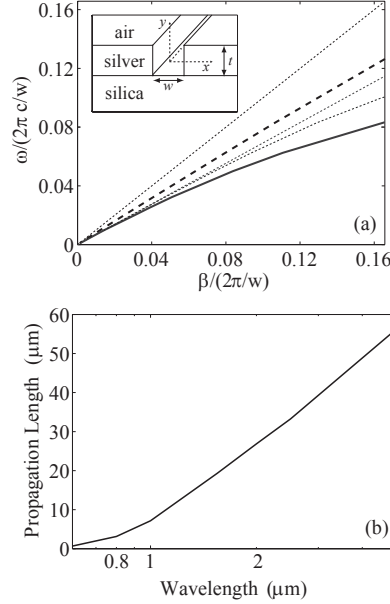


**Figure 2.** (a) Dispersion relation of the fundamental mode of the plasmonic slotline (shown with solid line) for  $w, t = 50$  nm (see inset) and of a PEC slotline (shown with dashed line). The upper, middle, and lower thin dotted curves are the light lines of air and silica and the lowest frequency mode of the silver film, respectively. (b) Propagation length of the fundamental mode of the plasmonic slotline as a function of wavelength for  $w, t = 50$  nm.

## 2.2. Dispersion relation of the plasmonic slotline mode

In Fig. 2a we show the dispersion relation of the fundamental mode of the plasmonic slotline. The width  $w$  and thickness  $t$  of the slot are 50 nm and the substrate material is silica ( $n_s = 1.44$ ). We observe that such a structure supports a bound mode in a wide frequency range. Within this range this mode has a wavevector larger than all radiation modes in air and silica, as well as all propagating modes in the air-silver-silica thin film structure. The cutoff frequency of this mode is  $\sim 0.005(2\pi c/w)$ , where  $c$  is the speed of light in free space. We also found that, if the slot dimensions are smaller than 100 nm, the optical communication frequency ( $\lambda_0 = 1.55\mu\text{m}$ ) is well above  $\omega_{\text{cutoff}}$ . Since the slot dimensions are much smaller than the wavelength in the frequency range of interest, the fundamental bound mode is quasi-TEM with dominant field components  $E_x$  and  $H_y$ , and this waveguide does not support any higher order bound modes. Since the fundamental mode is quasi-TEM, it can be efficiently excited by linearly polarized light.

As a comparison, in Fig. 2a we also show the dispersion relation when the perfect electric conductor (PEC) approximation is used for the metallic regions. We observe that the PEC slotline structure on substrate does not support a bound mode at any frequency. When the slot dimensions are far smaller than the wavelength, the fields are essentially the same as those of the static case.<sup>19</sup> In the PEC case, the fields do not penetrate into the metal. The field lines are either in air or in silica. The effective index of the mode  $n_{\text{eff}}$  therefore satisfies the relation  $1 < n_{\text{eff}} < n_s$ .<sup>19</sup> The PEC model is commonly used to describe slotlines at microwave frequencies. While such structures do not support any bound mode, in practice they guide waves effectively,<sup>19,20</sup> since radiation loss turns out to be negligible for deep subwavelength structures. In comparison, the existence of a bound mode for the plasmonic slotline is entirely due to the finite negative dielectric constant of metals at optical frequencies, which results in higher  $n_{\text{eff}}$  for the fundamental mode.

In Fig. 2b we show the propagation length  $L_p$  of the fundamental mode of the plasmonic slotline as a function of wavelength. The propagation length decreases as the wavelength decreases. This is due to the fact that the propagation length of surface plasmons scales with the wavelength,<sup>21</sup> since the fraction of the modal power in the metal increases at shorter wavelengths,<sup>9</sup> and also due to increased material losses of metals at shorter wavelengths.<sup>1</sup> At the optical communication wavelength of  $1.55\mu\text{m}$  the propagation length is  $\sim 20\mu\text{m}$ .

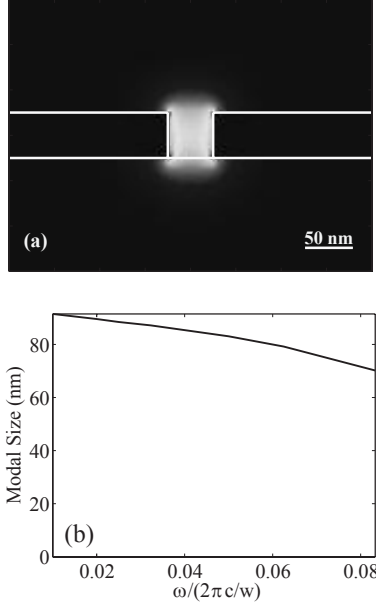


**Figure 3.** (a) Power density profile at  $\lambda_0 = 1.55\mu\text{m}$ , and (b) Modal size as a function of frequency of the fundamental mode of the plasmonic slotline for  $w, t = 50\text{ nm}$ .

### 2.3. Modal size

In Fig. 3a we show the power density profile of the fundamental mode of the plasmonic slotline for  $\lambda_0 = 1.55\mu\text{m}$ . We observe that the mode is mostly confined in the slot region and slightly extends in the adjacent silica and air regions. The maximum intensity is observed at the silver-air interfaces in the slot. This is expected since the mode can be seen as being formed by the coupling of the surface plasmon-polaritons at the two silver-air interfaces. In Fig. 3b we show the modal size, defined as the square root of the area in which the mode power density is larger than  $1/e^2$  of its maximum value, as a function of frequency. At the optical communication wavelength of  $1.55\mu\text{m}$  the modal size is  $\sim 87\text{ nm}$ , which is much smaller than the minimum achievable modal sizes with high-index-contrast dielectric waveguides. For comparison, the minimum achievable modal size with square silicon waveguides embedded in silica at  $\lambda_0 = 1.55\mu\text{m}$  is  $\sim 400\text{ nm}$ .<sup>22</sup> We also note that the modal size varies only weakly as a function of frequency.

We observe that the modal size remains small even at low frequencies where the dispersion relation approaches the silica light line. This behavior is fundamentally different from that of conventional dielectric waveguides. In conventional dielectric waveguides, the fields in the low-index cladding surrounding the high-index core decay exponentially with a decay constant  $\alpha = \frac{2\pi}{\lambda_0} \sqrt{n_{\text{eff}}^2 - n_{\text{clad}}^2}$ , where  $n_{\text{clad}}$  is the refractive index of the cladding region.<sup>23</sup> In these structures, the minimum confinement of a guided optical mode is  $\sim \lambda_0 / (2n_{\text{core}})$ , where  $n_{\text{core}}$  is the refractive index of the core region.<sup>4</sup> If the dimensions of the core are reduced far below  $\lambda_0 / (2n_{\text{core}})$ , the dispersion relation of the optical mode approaches the cladding light line ( $n_{\text{eff}} \rightarrow n_{\text{clad}}$ ), the decay constant  $\alpha$  becomes extremely small, and the modal size becomes extremely large.<sup>22, 23</sup> In contrast, in the case of the plasmonic slotline, even though the same exponential behavior should still hold in the far field, the modal size is dominated by the near field of the slot.

### 2.4. Near and far field characteristics of the plasmonic slotline mode

In Fig. 4a we show the power density profile of the fundamental mode of the plasmonic slotline in a vertical cut at  $x = 0$  (Fig. 2a) for  $w, t = 25\text{ nm}, 50\text{ nm}, 100\text{ nm}$  and  $\lambda_0 = 1.55\mu\text{m}$ . This profile has two distinctive characteristics related to the near and far fields. Far from the slot, the modal power density decays asymptotically as  $\sim \exp(-2\alpha\rho) / \rho$ , where  $\alpha = \text{Re} \sqrt{-\gamma^2 - (\frac{2\pi n_{\text{clad}}}{\lambda_0})^2}$ , as expected from Maxwell's equations. If the slot dimensions

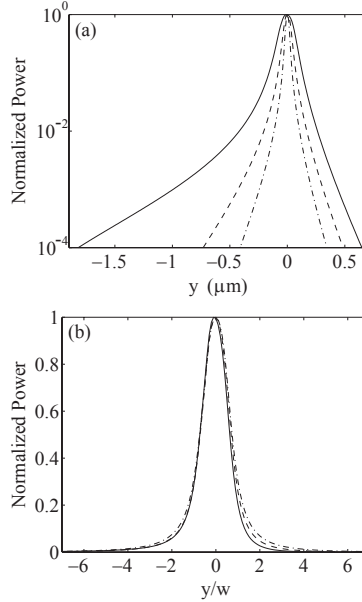


**Figure 4.** (a) Power density profile at  $\lambda_0 = 1.55\mu\text{m}$  of the fundamental mode of the plasmonic slotline at  $x = 0$  (Fig. 2a) for  $w, t = 25\text{nm}, 50\text{nm}, 100\text{nm}$  (shown with dash-dotted, dashed, and solid lines respectively). (b) Power density profile at  $x = 0$  in the vicinity of the slot for  $w, t = 25\text{nm}, 50\text{nm}, 100\text{nm}$ . Note that the horizontal axis is normalized with respect to  $w$ .

$w, t$  increase, the effective index of the mode  $n_{\text{eff}}$  decreases, and therefore, the decay rate  $\alpha$  decreases. Note also that, since  $n_s = 1.44 > 1$ , the decay rate is always larger in air.

In Fig. 4b we show the power density profile in the vicinity of the slot. We observe that the near field of the slot scales with the slot dimensions  $w, t$  and is independent of  $w/\lambda_0$ . This is due to the fact that the slot dimensions are much smaller than the wavelength. In addition, silver satisfies the condition  $|\epsilon_{\text{metal}}| \gg \epsilon_{\text{air}}$  at  $\lambda_0 \sim 1.55\mu\text{m}$ .<sup>1</sup> Thus, based on the boundary condition for the normal component of the electric field  $E_x$  at the silver-air interfaces in the slot, we have  $|E_{x \text{ metal}}| \ll |E_{x \text{ air}}|$ . The modal profile is therefore highly-confined in the slot region (Fig. 3a) and the modal size is dominated by the near field of the slot. Thus, even when the dispersion relation of the mode approaches the silica light line and the far-field decay rate  $\alpha$  decreases, the modal size remains relatively small (Fig. 3b). In addition, since the near field scales with the slot dimensions, the modal size of the plasmonic slotline can be further reduced, if the slot dimensions are reduced. We note that this comes at the cost of reduced propagation length.<sup>24</sup>

### 3. BENDS AND SPLITTERS IN SLOT-BASED PLASMONIC WAVEGUIDES

In this section, we investigate the performance of bends and power splitters in two-dimensional slot-based plasmonic waveguides. Waveguide bends and splitters are basic structures for optical interconnects and therefore essential components of optical integrated circuits.<sup>13,25</sup> Here, of particular interest is the regime where the dimensions of bends and splitters are much smaller than the propagation length of the optical mode. In this regime, the relevant question is whether these bends and splitters will induce reflection or excess absorption loss on top of the propagation loss in the waveguides.

To answer this question we calculate the transmission coefficient of bends and splitters and normalize it with respect to the transmission coefficient of a straight waveguide with the same length. We show that, even though the waveguides are lossy, bends and splitters with no *additional* loss can be designed over a wavelength range that extends from DC to near-infrared, if the slot width  $d$  is small enough. This range includes the optical communication wavelength of  $1.55\mu\text{m}$ . This remarkable effect is not observed in other light-guiding structures

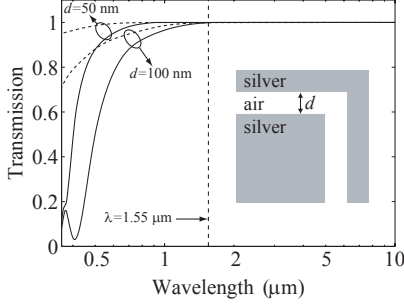


**Figure 5.** Transmission spectra of a MDM waveguide bend (shown in the inset) calculated using FDFD. We also show with dashed line the transmission spectra of a PEC parallel-plate waveguide bend. Results are shown for  $d = 50, 100$  nm. The vertical dashed line marks the optical communication wavelength of  $1.55\mu\text{m}$ .

such as high-index contrast or photonic crystal waveguides. We account for it with an effective characteristic impedance model based upon the real dispersion relation of the slot-based plasmonic waveguide structures.

We study the properties of silver-air-silver waveguide bends and splitters using a two-dimensional FDFD method.<sup>26, 27</sup> This method allows us to directly use experimental data for the frequency-dependent dielectric constant of silver,<sup>1</sup> including both the real and imaginary parts, with no further approximation. Perfectly matched layer (PML) absorbing boundary conditions are used at all boundaries.<sup>17</sup> We use a spatial grid size of  $2.5$  nm in FDFD which we found to be sufficient for convergence of numerical results.

### 3.1. Bends in slot-based plasmonic waveguides

To calculate the transmission coefficient of a  $90^\circ$  sharp slot-based plasmonic waveguide bend (inset of Fig. 5), we excite a dipole point source in the waveguide before the bend,<sup>28</sup> and measure the power flux of the transmitted optical mode after the bend. We perform a similar simulation in a straight waveguide and by comparing the two cases we extract the bending loss. In all cases  $d$  is much smaller than the wavelength so that only the fundamental TM waveguide mode (with magnetic field perpendicular to the direction of propagation) is excited. As an example, for  $d = 50$  nm the optical mode is fully formed  $\sim 20$  nm away from the source, the mode travels  $\sim 200$  nm before the bend, and the bent wave is measured  $\sim 200$  nm after the bend. In all cases the waveguide lengths in the simulations were chosen large enough to ensure correct calculation of the additional loss of bends. To validate our method, we used it to calculate the transmission coefficient of perfect electric conductor (PEC) parallel-plate waveguide bends and splitters and found excellent agreement with analytical results<sup>29, 30</sup> over the entire frequency range. In Fig. 5 we show the calculated bend transmission coefficient as a function of wavelength. We observe that at long wavelengths there is no bending loss. If the structure is small in comparison with the wavelength, the quasistatic approximation holds.<sup>31</sup> Under the quasistatic approximation, the bend is equivalent to a junction between two transmission lines with the same characteristic impedance, and there is therefore no bending loss. The limiting wavelength  $\lambda_c$  at which the transmission coefficient decreases below 99%, is  $1.27\mu\text{m}$  ( $0.76\mu\text{m}$ ) for  $d = 100$  nm ( $d = 50$  nm). The operating wavelength range widens as  $d$  decreases, because for thinner structures the quasistatic approximation holds over a wider range of wavelengths.

In Fig. 5 we also show the calculated transmission coefficient of the bending structures when the PEC approximation is used for the metallic regions. In a PEC parallel-plate waveguide, the transmission coefficient of a  $90^\circ$  bend is only a function of  $d/\lambda_0$ , i.e.  $T_{\text{PEC}} = T_{\text{PEC}}(d/\lambda_0)$ . If the device is small compared to the wavelength ( $d/\lambda_0 \ll 1$ ), there is no bending loss. The transmission coefficient decreases below 99% for  $d/\lambda_0 > 0.093$ . Thus, the limiting wavelength  $\lambda_c$  is  $1.08\mu\text{m}$  ( $0.54\mu\text{m}$ ) for  $d = 100$  nm ( $d = 50$  nm). We observe that the transmission spectra of the PEC parallel-plate waveguide bend and of the slot-based plasmonic waveguide bend differ significantly. The limiting wavelength  $\lambda_c$  is lower in the PEC case.

In order to interpret the difference between the PEC and plasmonic transmission spectra, we calculated the guide wavelength  $\lambda_g$  of the fundamental TM mode in the slot-based plasmonic waveguide. The guide wavelength  $\lambda_g$ , defined as  $\lambda_g \equiv 2\pi/\beta_{\text{pl}}$ , where  $\beta_{\text{pl}}$  is the real part of the mode propagation constant,<sup>31</sup> is calculated using

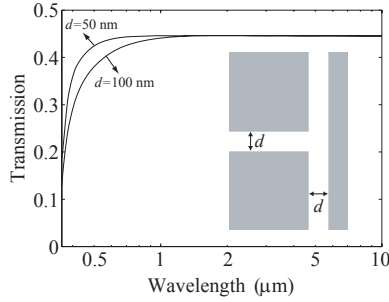


**Figure 6.** Calculated transmission spectra of a MDM  $T$ -shaped splitter (shown in the inset). Results are shown for  $d = 50, 100$  nm.

FDFD by exciting the fundamental mode in a straight slot-based plasmonic waveguide with a dipole source. To validate our method, we compared our results with results obtained by directly solving the dispersion relation of the slot-based plasmonic waveguide and found excellent agreement.<sup>32</sup> The calculated guide wavelength  $\lambda_g$  of the fundamental TM mode in the slot-based plasmonic waveguide is smaller than the free-space wavelength  $\lambda_0$ , which is the guide wavelength of the TEM mode in the PEC waveguide. Since  $\lambda_g < \lambda_0$ , the PEC waveguide structure is “smaller” (in comparison to the optical mode wavelength) than the slot-based plasmonic waveguide structure, and this can explain the lower  $\lambda_c$  in the PEC case. We actually found that the transmission spectra of the slot-based plasmonic waveguide bend  $T_{pl}$  is well approximated by the spectra of the PEC waveguide bend  $T_{PEC}$ , if the difference between  $\lambda_g$  and  $\lambda_0$  is taken into account, i.e.  $T_{pl} \simeq T_{PEC}(d/\lambda_g)$ . This approximation typically holds for  $\lambda \geq \lambda_c$ , where the bending loss of the slot-based plasmonic waveguide is dominated by reflection. At shorter wavelengths the bending loss is dominated by excess absorption and therefore this approximation no longer holds.

### 3.2. Splitters in slot-based plasmonic waveguides

We also calculate the transmission spectra of slot-based plasmonic splitters. The calculation method using FDFD is similar to the one described above for the  $90^\circ$  bend. In Fig. 6 we show the calculated transmission coefficient as a function of wavelength for a slot-based plasmonic  $T$ -shaped splitter (inset of Fig. 6). The frequency response of the slot-based plasmonic splitter is quite similar to the response of the slot-based plasmonic bend. At long wavelengths the transmission is equal to 44.4%. Under the quasistatic approximation, which holds at long wavelengths, the splitter is equivalent to a junction of three transmission lines with the same characteristic impedance  $Z_0$ . The load connected to the input transmission line at the junction consists of the series combination of the two output transmission lines. Thus, the equivalent load impedance is  $Z_L = 2Z_0$  and the reflection coefficient is  $R = |(Z_L - Z_0)/(Z_L + Z_0)|^2 = 1/9$ . Because of the symmetry of the structure, the transmitted optical power is equally distributed between the two output waveguide branches, so that the transmission coefficient is  $T = 4/9$ . As in the slot-based plasmonic bend, the operating wavelength range widens as  $d$  decreases. At  $\lambda \simeq \lambda_c$  the splitter loss is dominated by reflection, while at shorter wavelengths it is dominated by excess absorption.

### 3.3. Characteristic impedance of slot-based plasmonic waveguides

Based on the above discussion, in order to improve the transmission coefficient of the slot-based plasmonic splitter, we can adjust the characteristic impedance of the input waveguide  $Z_{in}$  so that  $Z_{in} \simeq Z_L = 2Z_0$ . The input impedance  $Z_{in}$  can be adjusted by varying the thickness  $d_{in}$  of the input waveguide. In Fig. 7 we show the calculated reflection coefficient  $R$  of the slot-based plasmonic  $T$ -shaped splitter at  $\lambda_0 = 1.55\mu\text{m}$  as a function of  $d_{in}/d_{out}$ , where  $d_{out} = 50$  nm is the thickness of the two output waveguide branches (inset of Fig. 7). We note that at  $\lambda_0 = 1.55\mu\text{m}$  the propagation length of the fundamental mode of the plasmonic waveguide is much larger than the splitter dimensions so that the contribution of excess absorption to the splitter loss is negligible. We observe that the reflection coefficient is below 1% for  $1.8 < d_{in}/d_{out} < 2.8$  and is minimized for  $d_{in}/d_{out} \simeq 2.25$ . We also

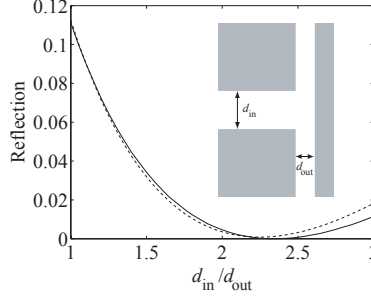


**Figure 7.** Reflection coefficient  $R$  of a MDM  $T$ -shaped splitter (shown in the inset) as a function of  $d_{\text{in}}/d_{\text{out}}$  at  $\lambda_0 = 1.55\mu\text{m}$  calculated using FDFD. We also show with dashed line the reflection coefficient  $\bar{R}$  calculated based on the characteristic impedance  $Z_{\text{MDM}}$  and transmission-line theory. Results are shown for  $d_{\text{out}} = 50\text{ nm}$ .

found that the limiting wavelength  $\lambda_c$  of the optimized splitter is almost the same as the limiting wavelength  $\lambda_c$  of the symmetric splitter of Fig. 6.

The characteristic impedance of the fundamental TEM mode in a PEC parallel-plate waveguide is uniquely defined as the ratio of voltage  $V$  to surface current density  $I$  and is equal to<sup>31</sup>

$$Z_{\text{TEM}} \equiv \frac{V}{I} = \frac{E_x d}{H_y} = \frac{\beta_{\text{TEM}} d}{\omega \epsilon_0} = \sqrt{\frac{\mu_0}{\epsilon_0}} d$$

where  $E_x$ ,  $H_y$  are the transverse components of the electric and magnetic field respectively, and we assumed a unit-length waveguide in the  $y$  direction. For non-TEM modes, such as the fundamental mode of the plasmonic waveguide, voltage and current are not uniquely defined. However, metals like silver satisfy the condition  $|\epsilon_{\text{metal}}| \gg \epsilon_{\text{diel}}$  at the optical communication wavelength of  $1.55\mu\text{m}$ .<sup>1</sup> Thus,  $|E_{x\text{ metal}}| \ll |E_{x\text{ diel}}|$  so that the integral of the electric field in the transverse direction can be approximated by  $E_{x\text{ diel}} d$  and we may therefore define the characteristic impedance of the fundamental mode of the plasmonic waveguide as

$$Z_{\text{pl}}(d) \equiv \frac{E_{x\text{ diel}} d}{H_{y\text{ diel}}} = \frac{\beta_{\text{pl}}(d)}{\omega \epsilon_0} d$$

where  $\beta_{\text{pl}}(d) = 2\pi/\lambda_g(d)$ , and the guide wavelength  $\lambda_g$  is calculated as mentioned above. In Fig. 7 we show the reflection coefficient of the slot-based plasmonic  $T$ -shaped splitter calculated based on  $Z_{\text{pl}}$  as

$$\bar{R} = \left| \frac{Z_L - Z_0}{Z_L + Z_0} \right|^2 = \left| \frac{2Z_{\text{pl}}(d_{\text{out}}) - Z_{\text{pl}}(d_{\text{in}})}{2Z_{\text{pl}}(d_{\text{out}}) + Z_{\text{pl}}(d_{\text{in}})} \right|^2$$

We observe that there is very good agreement between  $\bar{R}$  and the exact reflection coefficient  $R$  calculated using FDFD. This agreement suggests that the concept of characteristic impedance for slot-based plasmonic waveguides is indeed valid and useful. The deviation between  $\bar{R}$  and  $R$  at large values of  $d_{\text{in}}/d_{\text{out}}$  is due to the fact that  $d_{\text{in}}$  is not very small compared to the wavelength and the quasistatic approximation therefore breaks down. We found that similar deviations are observed for PEC parallel-plate waveguides. Such deviations decrease at longer wavelengths in both the PEC and slot-based plasmonic waveguide cases.

As final remarks, we expect that the impedance concept can be generalized to three-dimensional slot-based plasmonic waveguides when the dielectric layer thickness is much smaller than the wavelength. Finally we note that, even though the choice of metal affects the propagation length of slot-based plasmonic waveguides,<sup>24</sup> our conclusions on bends and splitters are valid regardless of the choice of metal.

## ACKNOWLEDGMENTS

This research was supported by DARPA/MARCO under the Interconnect Focus Center and by AFOSR grant FA 9550-04-1-0437.

## REFERENCES

1. E. D. Palik, *Handbook of Optical Constants of Solids*, Academic, New York, 1985.
2. A. Taflove, *Computational Electrodynamics*, Artech House, Boston, 1995.
3. A. D. Rakic, A. B. Djuricic, J. M. Elazar, and M. L. Majewski, "Optical properties of metallic films for vertical-cavity optoelectronic devices," *Appl. Opt.* **37**, pp. 5271–5283, 1998.
4. J. Takahara, S. Yamagishi, H. Taki, A. Morimoto, and T. Kobayashi, "Guiding of a one-dimensional optical beam with nanometer diameter," *Opt. Lett.* **22**, pp. 475–477, 1997.
5. V. R. Almeida, Q. F. Xu, C. A. Barrios, and M. Lipson, "Guiding and confining light in void nanostructure," *Opt. Lett.* **29**, pp. 1209–1211, 2004.
6. J. J. Burke, G. I. Stegeman, and T. Tamir, "Surface-polariton-like waves guided by thin, lossy metal films," *Phys. Rev. B* **33**, pp. 5186–5201, 1986.
7. J. C. Weeber, A. Dereux, C. Girard, J. R. Krenn, and J. P. Goudonnet, "Plasmon polaritons of metallic nanowires for controlling submicron propagation of light," *Phys. Rev. B* **60**, pp. 9061–9068, 1999.
8. J. R. Krenn, B. Lamprecht, H. Ditlbacher, G. Schider, M. Salerno, A. Leitner, and F. R. Aussenegg, "Non-diffraction-limited light transport by gold nanowires," *Europhys. Lett.* **60**, pp. 663–669, 2002.
9. P. Berini, "Plasmon-polariton waves guided by thin lossy metal films of finite width: Bound modes of symmetric structures," *Phys. Rev. B* **61**, pp. 10484–10503, 2000.
10. M. L. Brongersma, J. W. Hartman, and H. A. Atwater, "Electromagnetic energy transfer and switching in nanoparticle chain arrays below the diffraction limit," *Phys. Rev. B* **62**, pp. R16356–R16359, 2000.
11. S. A. Maier, P. G. Kik, H. A. Atwater, S. Meltzer, E. Harel, B. E. Koel, and A. A. G. Requicha, "Local detection of electromagnetic energy transport below the diffraction limit in metal nanoparticle plasmon waveguides," *Nat. Mater.* **2**, pp. 229–232, 2003.
12. F. Kusunoki, T. Yotsuya, J. Takahara, and T. Kobayashi, "Propagation properties of guided waves in index-guided two-dimensional optical waveguides," *Appl. Phys. Lett.* **86**, p. 211101, 2005.
13. K. Tanaka and M. Tanaka, "Simulations of nanometric optical circuits based on surface plasmon polariton gap waveguide," *Appl. Phys. Lett.* **82**, pp. 1158–1160, 2003.
14. I. V. Novikov and A. A. Maradudin, "Channel polaritons," *Phys. Rev. B* **66**, pp. 035403–035413, 2002.
15. D. F. P. Pile and D. K. Gramotnev, "Channel plasmon-polariton in a triangular groove on a metal surface," *Opt. Lett.* **29**, pp. 1069–1071, 2004.
16. J. A. Pereda, A. Vegas, and A. Prieto, "An improved compact 2d full-wave fdtd method for general guided wave structures," *Microwave Opt. Tech. Lett.* **38**, pp. 331–335, 2003.
17. J. Jin, *The Finite Element Method in Electromagnetics*, John Wiley & Sons, New York, 2002.
18. S. J. Al-Bader, "Optical transmission on metallic wires-fundamental modes," *IEEE J. Quantum Electron.* **40**, pp. 325–329, 2004.
19. D. M. Pozar, *Microwave Engineering*, Wiley, New York, 1998.
20. E. A. Mariani, C. P. Heinzman, J. P. Agrios, and S. B. Cohn, "Slot line characteristics," *IEEE Trans. Microwave Theory Tech.* **17**, pp. 1091–1096, 1969.
21. W. L. Barnes, A. Dereux, and T. W. Ebbesen, "Surface plasmon subwavelength optics," *Nature* **424**, pp. 824–830, 2003.
22. L. Vivien, S. Laval, E. Cassan, X. L. Roux, and D. Pascal, "2-d taper for low-loss coupling between polarization-insensitive microwaveguides and single-mode optical fibers," *J. Lightwave Technol.* **21**, pp. 2429–2433, 2003.
23. S. L. Chuang, *Physics of Optoelectronic Devices*, Wiley, New York, 1995.
24. R. Zia, M. D. Selker, P. B. Catrysse, and M. L. Brongersma, "Geometries and materials for subwavelength surface plasmon modes," *J. Opt. Soc. Am. A* **21**, pp. 2442–2446, 2004.
25. C. Manolatu, S. G. Johnson, S. Fan, P. R. Villeneuve, H. A. Haus, and J. D. Joannopoulos, "High-density integrated optics," *J. Lightwave Technol.* **17**, pp. 1682–1692, 1999.
26. S. D. Wu and E. N. Glytsis, "Finite-number-of-periods holographic gratings with finite-width incident beams: analysis using the finite-difference frequency-domain method," *J. Opt. Soc. Am. A* **19**, pp. 2018–2029, 2002.

27. G. Veronis, R. W. Dutton, and S. Fan, "Method for sensitivity analysis of photonic crystal devices," *Opt. Lett.* **29**, pp. 2288–2290, 2004.
28. A. Mekis, J. C. Chen, I. Kurland, S. H. Fan, P. R. Villeneuve, and J. D. Joannopoulos, "High transmission through sharp bends in photonic crystal waveguides," *Phys. Rev. Lett.* **77**, pp. 3787–3790, 1996.
29. N. Marcuvitz, *Waveguide Handbook*, McGraw-Hill, New York, 1951.
30. K. H. Park, H. J. Eom, and Y. Yamaguchi, "An analytic series solution for e-plane t-junction in parallel-plate waveguide," *IEEE Trans. Microwave Theory Tech.* **42**, pp. 356–358, 1994.
31. S. Ramo, J. R. Whinnery, and T. V. Duzer, *Fields and Waves in Communication Electronics*, Wiley, New York, 1994.
32. H. Shin, M. F. Yanik, S. H. Fan, R. Zia, and M. L. Brongersma, "Omnidirectional resonance in a metal-dielectric-metal geometry," *Appl. Phys. Lett.* **84**, pp. 4421–4423, 2004.